Eur. Phys. J. B **17**, 411–415 (2000)

THE EUROPEAN PHYSICAL JOURNAL B

EDP Sciences

Phase diagram of the three-dimensional Hubbard model at half filling

R. Staudt[1], M. Dzierzawa[1,a], and A. Muramatsu[2]

[1] Institute of Physics, University of Augsburg, Universitätsstraße 1, 86135 Augsburg, Germany
[2] Institute of Physics, University of Stuttgart, Pfaffenwaldring 57, 70550 Stuttgart, Germany

Received 11 April 2000 and Revised in final form 29 June 2000

Abstract. We investigate the phase diagram of the three-dimensional Hubbard model at half filling using quantum Monte Carlo (QMC) simulations. The antiferromagnetic Néel temperature $T_{\rm N}$ is determined from the specific heat maximum in combination with finite-size scaling of the magnetic structure factor. Our results interpolate smoothly between the asymptotic solutions for weak and strong coupling, respectively, in contrast to previous QMC simulations. The location of the metal-insulator transition in the paramagnetic phase above $T_{\rm N}$ is determined using the electronic compressibility as criterion.

PACS. 71.10.Fd Lattice fermion models (Hubbard model, etc.) – 71.10.Hf Non-Fermi-liquid ground states, electron phase diagrams and phase transitions in model systems – 71.30.+h Metal-insulator transitions and other electronic transitions

1 Introduction

The canonical lattice model for correlated electrons is the Hubbard model [1–3] defined by the Hamiltonian

$$\hat{H} = -t \sum_{<ij>,\sigma} (\hat{c}^{\dagger}_{i\sigma}\hat{c}_{j\sigma} + \hat{c}^{\dagger}_{j\sigma}\hat{c}_{i\sigma}) + U \sum_{i} \hat{n}_{i\uparrow}\hat{n}_{i\downarrow} \quad (1)$$

where $\hat{c}^{\dagger}_{i\sigma}$ ($\hat{c}_{i\sigma}$) are electron creation (annihilation) operators, $\langle ij\rangle$ denotes a pair of neighboring lattice sites and t and U are the hopping matrix element and the onsite Coulomb energy, respectively. At half filling the ground state of the 3D Hubbard model on a simple cubic lattice has antiferromagnetic long range order for all positive values of U due to the perfect nesting of the Fermi surface. At finite temperatures the sublattice magnetization is reduced by thermal fluctuations and a transition to a paramagnetic phase occurs at the Néel temperature $T_{\rm N}$. In the strong coupling limit the energy scale for magnetism is obtained by mapping the Hubbard model to the antiferromagnetic spin 1/2 Heisenberg model with exchange coupling $J = 4\,t^2/U$. For small U antiferromagnetism results from the Fermi surface instability and the relevant energy scale is set by the BCS like expression $T_{\rm N} \propto t\exp(-1/(\rho_0 U))$ where ρ_0 is the density of states at the band center.

There have been many attempts to calculate $T_{\rm N}$ over the whole range of U using both QMC simulations [4–6] and analytical approaches including variational methods [7], Hartree Fock theory [8], strong coupling expansions [9], dynamical mean field theory (DMFT) [10–12], the two-particle self-consistent formalism [13] and spin fluctuation theory [14]. A critical comparison of the various approaches can be found in references [9,13]. A common drawback of mean-field like approximations is that in the strong coupling limit they fail to reproduce the correct Heisenberg result $T_{\rm N} = 3.83\,t^2/U$ [15] and instead reduce to the Weiss molecular field theory with $T_{\rm N}^{\rm mf} = 6\,t^2/U$. Strong coupling expansions, on the other hand, break down in the Fermi surface instability regime. As to numerical methods, the results of previous QMC simulations [4,5] do not agree with each other and have been questioned by Hasegawa [16] who argued that they overestimate $T_{\rm N}$ considerably. Nevertheless, for lack of alternatives the QMC results of references [4,5] have served as benchmarks for analytical approaches over the last ten years despite the controversy concerning their reliability. Clearly, there is need for improved QMC simulations of the 3D Hubbard model with better statistics and for larger systems than previously accessible.

Besides antiferromagnetism the second important phenomenon described by the half-filled Hubbard model is the interaction-induced metal-insulator transition, known as Mott-Hubbard transition [17]. This transition occurs when the ratio of the interaction strength U and the bandwidth W exceeds some critical value of order one. Unfortunately, the presence of antiferromagnetic order makes it impossible to observe the Mott-Hubbard transition in the 3D Hubbard model at temperatures below

[a] e-mail: michael.dzierzawa@physik.uni-augsburg.de

T_N. DMFT calculations for the fully frustrated Hubbard model [18] where antiferromagnetism is completely suppressed predict a first order metal-insulator transition line that persists up to a critical point at (U_c, T_c) in the phase diagram, followed by a crossover region above this critical point. In this paper we examine if such a first order transition line can also be observed in the 3D Hubbard model or if it is completely occluded by the antiferromagnetic phase below T_N.

2 Magnetic phase transition

We have studied the 3D Hubbard model on a simple cubic lattice with periodic boundary conditions using a finite temperature, grand canonical QMC algorithm [19,20] which is based on a discrete Hubbard-Stratonovich decoupling of the Hubbard interaction term. In this algorithm, the inverse temperature or imaginary time β has to be divided into a finite number of steps $\Delta\tau$ which introduces an error $\propto \Delta\tau^2 tU$ into the calculations. We have chosen $\Delta\tau^2 tU = 0.1$ after making sure that the results are not significantly affected by the extrapolation $\Delta\tau \to 0$. A typical simulation on a $L \times L \times L$ lattice consisted of between 100 000 ($L = 4$) and 2 000 ($L = 10$) measurement sweeps that were grouped into 20 blocks in order to estimate the statistical error of the QMC data. QMC simulations frequently suffer from the minus sign problem, *i.e.* the fact that the fermionic determinant that serves as probability weight function is not always positive, in particular at low temperatures. At half filling where most of our simulations were performed this problem does not exist due to particle-hole symmetry, but even in the calculations of the compressibility that require simulations away from half filling we never encountered any serious minus sign problem since we worked at relatively high temperatures.

Our first goal is to determine the antiferromagnetic Néel temperature as function of the interaction strength U. To this end we have calculated the specific heat which is the central quantity to characterize thermodynamical properties of many-particle systems and is easily accessible both experimentally and from numerical simulations. Since phase transitions are usually accompanied by a maximum or a divergence of the specific heat the transition temperature can be determined from specific heat data without measuring the order parameter directly. Of course, not every maximum of the specific heat is associated with a phase transition; one has to verify that the order parameter indeed changes from zero to a nonzero value at the presumed transition temperature. In the Hubbard model for sufficiently large U there are two maxima of the specific heat, one at low temperatures $\propto t^2/U$ reflecting spin excitations, the second on a higher energy scale $\propto U$ associated with charge excitations. Here we concentrate on the low temperature peak which we use to determine the Néel temperature.

The specific heat can either be calculated *via* $C = \partial E/\partial T$ or from the energy fluctuations, $C \propto \langle \hat{H}^2 \rangle - \langle \hat{H} \rangle^2$. We employ the first method which turns out to be numerically more accurate. The following procedure is used: First the energy is calculated with QMC in a temperature range where the phase transition is expected to take place. The simulations are performed at fixed imaginary time slice $\Delta\tau$ for all temperatures. An extrapolation $\Delta \to 0$ is not necessary since the finite $\Delta\tau$ corrections to the energy are nearly temperature independent over the relatively small temperature range under consideration and even taking into account corrections to linear order in T does not affect the position of the specific heat maximum. In order to calculate the specific heat from the energy data the temperature interval is divided in a number of equidistant values. For each of these temperatures T_i the value of the specific heat C_i is determined such, that i) the resulting curve is as smooth as possible and ii) the energies $E_{\rm fit}$ obtained by numerical integration of the specific heat values C_i are as close as possible to the QMC data. In practice this is achieved by minimizing the quantity $\lambda_1 A + \lambda_2 B$ where $A = \sum_i (C_{i+1} - 2C_i + C_{i-1})^2$ controls the smoothness of the fit while $B = \sum((E_{\rm fit} - E_{\rm QMC})/\sigma_{\rm QMC})^2$ measures the deviation between the fit and the QMC data. This procedure avoids to chose a specific functional form for the fit function which could bias the results in some way or the other. The ratio of the parameters λ_1 and λ_2 is fixed such that the energy values obtained by the minimization procedure lie within the statistical errors $\sigma_{\rm QMC}$ of the QMC data. We have checked that the final results are very robust against moderate variations of the ratio λ_1/λ_2. In order to estimate the error bars for the specific heat we have performed an average over many different input energy data sets obtained by adding random noise of the order of $\sigma_{\rm QMC}$ to the mean values $E_{\rm QMC}$. Of course, any noise-reducing algorithm tends to wash out sharp structures like cusps or discontinuities. On the other hand, the specific heat curves obtained from extensive QMC simulations of the three-dimensional spin 1/2 Heisenberg model [21] are as smooth as ours indicating that there exist no sharp structures that could be lost by the procedure that we use to calculate the specific heat, at least for the system sizes that we consider. In any case, the location of the maximum which we are mainly interested in is only very little affected.

Figure 1 shows the energy as function of temperature for $L = 4$ and several values of U. Here and in the following figures we have fixed the energy scale by setting $t = 1$. The curves connecting the data are obtained with the fitting procedure described above. They all have a point of inflection indicating that the specific heat maxima are contained in the respective temperature intervals. In Figure 2 the specific heat for $U = 6$ is displayed as function of temperature for $L = 4, 6, 8$ and 10. The maximum value of C increases somewhat with increasing system size while simultaneously the position of the maximum $T_{\rm max}$ is slightly shifted to lower temperatures. There is no indication of a divergence for large systems. This is in agreement with the assumption that the half-filled Hubbard model belongs to the 3D Heisenberg universality class with a negative exponent $\alpha \approx -0.11$ which means that the specific heat

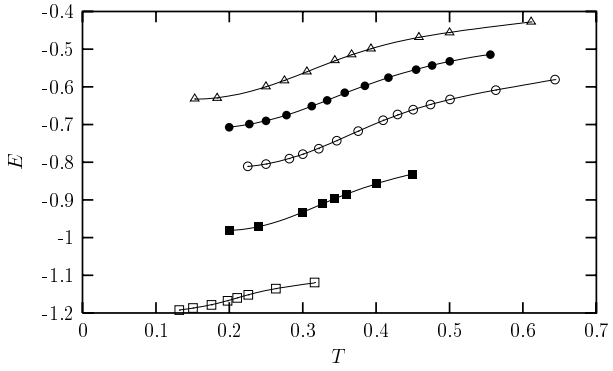

Fig. 1. Energy as function of temperature for $L = 4$ and $U = 4, 6, 8, 10, 12$ (from bottom to top). Error bars are much smaller than the size of the symbols. The curves are obtained with the procedure described in the text.

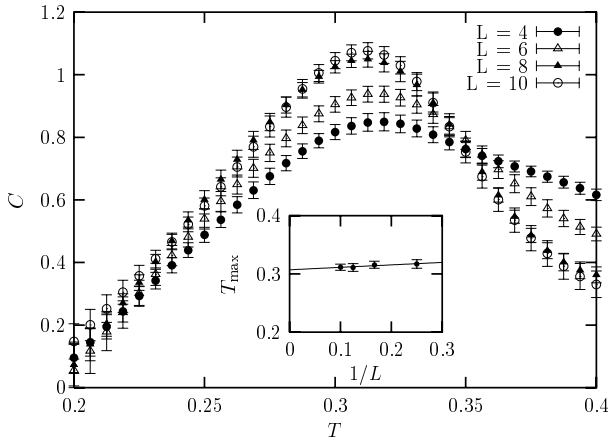

Fig. 2. Specific heat as function of temperature for $U = 6$ and $L = 4, 6, 8, 10$. The inset shows the position of the maximum of the specific heat *vs.* $1/L$.

has only a cusp but no divergence at the critical temperature. High precision QMC simulations of the 3D spin 1/2 Heisenberg model [21] confirm this behavior. In the Heisenberg model the shift of the maximum of C between $L = 4$ and the infinite lattice is about five percent. In the inset of Figure 2 the peak temperature $T_{\max}$ is plotted *vs.* $1/L$ indicating that in the Hubbard model finite-size corrections are quite small as well. A linear fit yields $T_{\rm N} = 0.31 \pm 0.01$.

We now demonstrate that the peaks in the specific heat are indeed associated with the antiferromagnetic phase transition. To this end we have calculated the magnetic structure factor

$$S(\mathbf{Q}) = \frac{1}{L^3} \sum_{i,j} \mathrm{e}^{\mathrm{i}\,\mathbf{Q}\,(\mathbf{R}_i - \mathbf{R}_j)} \langle (\hat{n}_{i\uparrow} - \hat{n}_{i\downarrow})(\hat{n}_{j\uparrow} - \hat{n}_{j\downarrow}) \rangle \quad (2)$$

where $\mathbf{Q} = (\pi, \pi, \pi)$ is the antiferromagnetic wave vector. $S(\mathbf{Q})$ is related to the sublattice magnetization m *via*

$$\frac{S(\mathbf{Q})}{L^3} = m^2 + f(L) \quad (3)$$

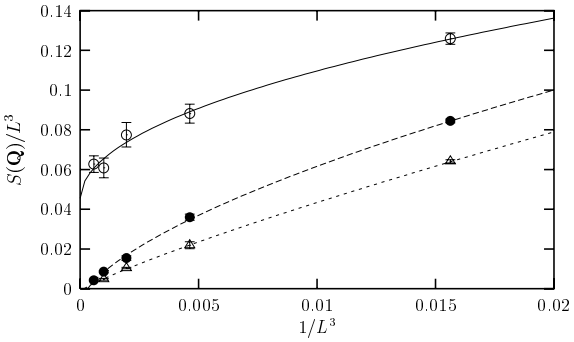

Fig. 3. Finite size scaling of the magnetic structure factor for $U = 6$ and $T = 0.3, 0.36$ and 0.4 (from top to bottom).

where $f(L) \to 0$ for $L \to \infty$. In order to extrapolate the finite lattice QMC data to the thermodynamic limit one has to know the asymptotic behavior of $f(L)$ for large L. Right at the critical temperature the structure factor $S(\mathbf{Q})$ should scale with the system size as $L^{2-\eta}$ where $\eta \approx 0.03$ for the 3D Heisenberg universality class [21] and therefore $f(L) \propto L^{-1.03}$. In the ordered phase at low temperatures, spin wave theory predicts $f(L) \propto L^{-2}$ assuming a linear magnon dispersion. On the other hand, in the paramagnetic phase above $T_{\rm N}$ spin correlations decay exponentially and we expect $f(L) \propto L^{-3}$ provided the correlation length is smaller than the system size. In order to take into account all these possibilities we have extrapolated our QMC data using $f(L) \propto L^{-\lambda}$ where λ itself is a fit parameter. Since the asymptotic behavior of $f(L)$ is only reached for sufficiently large lattices we have checked that the omission of the data for small lattices ($L = 4$ and $L = 6$) does not lead to different conclusions concerning the existence or absence of antiferromagnetic long range order.

The results of such a finite-size extrapolation are displayed in Figure 3 for $U = 6$ and $T = 0.3, 0.36$ and 0.4. While the curves for the two higher temperatures extrapolate to a value close to zero indicating the absence of long-range order, the curve for $T = 0.3$ yields a finite value corresponding to a finite sublattice magnetization. This behavior is in agreement with the value $T_{\rm N} \approx 0.31$ that we have extracted from the specific heat data. Preliminary results concerning the magnetic structure factor for other values of U have been published elsewhere [22]. A more comprehensive presentation including computational details can be found in [23].

We summarize our results concerning the magnetic phase transition in Figure 4 where the Néel temperature of the 3D Hubbard model obtained from different methods is displayed as function of U. For comparison the asymptotic behavior in the weak and strong coupling limit is also shown. In Hartree Fock theory, applicable for small U, $T_{\rm N}$ is determined by the gap equation

$$\frac{2}{U} = \int \mathrm{d}\epsilon \, \frac{\rho(\epsilon)}{\epsilon} \, \tanh \frac{\epsilon}{2T_{\rm N}} \quad (4)$$

where $\rho(\epsilon)$ is the density of states. As pointed out by van Dongen [8] the true asymptotic Néel temperature

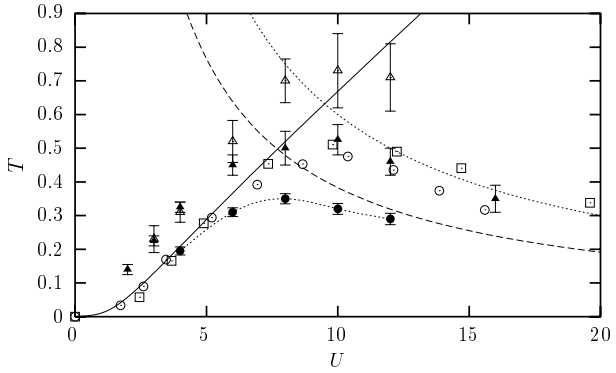

Fig. 4. Magnetic phase diagram of the half-filled Hubbard model. Néel temperature $T_{\rm N}$ as function of U from various approaches: QMC, this work (filled circles; dots are meant as a guide to the eye only), QMC [4] (open triangles), QMC [5] (filled triangles), DMFT [10] (open circles), DMFT [12] (open squares), modified Hartree-Fock theory [8] (solid curve), Heisenberg limit from high temperature expansions, $T_{\rm N} = 3.83t^2/U$ [15] (dashed curve), Weiss molecular field theory, $T_{\rm N}^{\rm mf} = 6t^2/U$ (dotted curve).

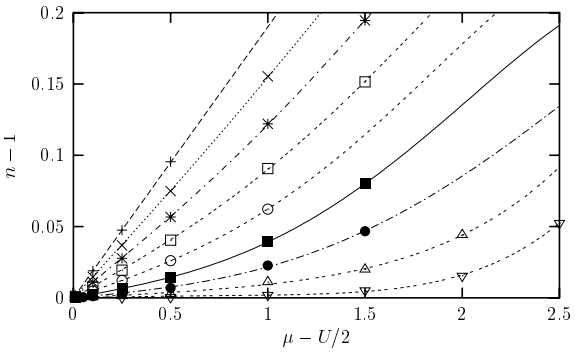

Fig. 5. Particle density n as function of the chemical potential μ for $U = 3, 4, 5, 6, 7, 8, 9, 10, 12$ (from top to bottom), $T = 0.45$ and $L = 4$. The curves are polynomial fits.

in the weak coupling limit is reduced by a factor $q \approx 0.282$ compared to the solution of (4). We have included this reduction factor in the curve shown in the figure. In the strong coupling limit the Hubbard model can be mapped to the spin 1/2 Heisenberg model where the critical temperature is known from high temperature series [15] and QMC simulations [21] which yield $T_{\rm N} = 3.83t^2/U$, compared to the Weiss molecular field result $T_{\rm N}^{\rm mf} = 6t^2/U$. Our QMC results interpolate smoothly between weak and strong coupling asymptotics whereas the old QMC data of references [4,5] are clearly off in both limits.

Comparing our results with DMFT data is not straightforward since in DMFT calculations mostly a Gaussian or a semi-elliptic density of states is used which both differ from the non-interacting density of states of the 3D Hubbard model. To convert energies we have expressed the hopping matrix element t (which is our energy unit) in terms of the second moment of the density of states *via* $t = \sqrt{\langle \epsilon^2 \rangle / 6}$. In practice this means that the energy data from reference [10] have been multiplied by a factor $2\sqrt{3}$ and those from reference [12] by a factor of $2\sqrt{6}$. In the weak coupling regime $U \lesssim 6$ there is good agreement between the DMFT results and our QMC data while for intermediate and large values of U the DMFT yields substantially higher values of $T_{\rm N}$. This is not surprising since in the limit $U \to \infty$ the DMFT reduces to the Weiss molecular field theory of the Heisenberg model. There are however significant discrepancies between the DMFT data from references [10,12] for large U. This might be due to the fact that in the first case a Gaussian and in the latter a semi-elliptic density of states was used. It should also be noted that the DMFT data from [12] approach the molecular field limit from above while the curve of [10] and also our QMC data lie always below their respective strong coupling asymptote.

3 Metal insulator transition

At a true metal insulator transition the DC conductivity σ drops to zero when some control parameter is changed across a critical value. This is strictly speaking only possible at zero temperature whereas for $T > 0$ the conductivity remains always finite due to thermal activation. Unfortunately, the DC conductivity – although quite easily accessible in experiment – is very hard to obtain from QMC simulations, since the required analytic continuation of the current-current correlation function from Matsubara to real frequencies is numerically a very hard problem when the input data are noisy. We have therefore based our considerations on calculations of the electronic compressibility $\kappa = \partial n / \partial \mu$ which can be obtained with high accuracy from QMC simulations. Although there is no simple relation between σ and κ both are expected to be finite in the metallic and exponentially small in the insulating regime.

DMFT calculations employing the iterated perturbation theory [18] have revealed the following scenario for the Mott Hubbard transition. In the fully frustrated Hubbard model there exists a first-order metal-insulator transition line due to a coexistence regime of metallic and insulating solutions at low temperatures. This first order line ends at a critical point, reminiscent of an ordinary liquid gas transition [24]. Recent numerical work has corroborated this scenario. In fact, the first order transition can also be observed as a jump in the average number of doubly occupied sites [24] and it is expected that the compressibility is discontinuous as well.

Figure 5 shows how the particle density n depends on the chemical potential μ for $T = 0.45$ which is slightly above the antiferromagnetic phase boundary. Due to particle-hole symmetry $n - 1$ is an odd function of $\mu - U/2$. We have therefore used the polynomial $f(x) = ax + bx^3 + cx^5$ to fit the QMC data. The coefficient a yields the compressibility κ which is displayed as function of U in Figure 6. There is no sign of a discontinuity as should be observed in the case of a first order transition. Instead the compressibility decreases smoothly up to $U \approx 8$ and can be very accurately approximated by a second order polynomial in this range, as indicated

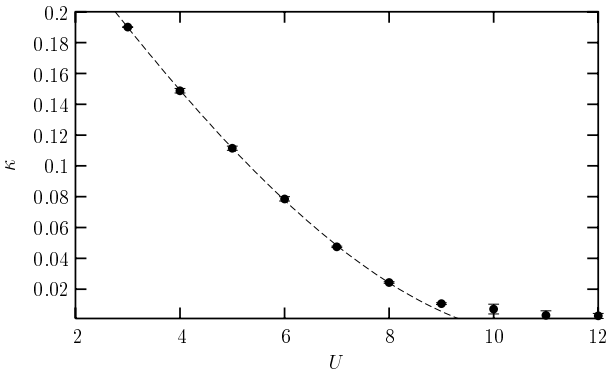

Fig. 6. Electronic compressibility κ as function of U. The curve is a polynomial fit for the range $3 < U < 8$.

by the dashed curve in the figure. Afterwards it turns over into an exponential-like tail that we associate with the crossover regime where only thermal activation across the gap contributes to the compressibility. Unfortunately our data are not precise enough to extract the U dependence of the gap. The observation of a crossover regime instead of a true metal-insulator transition is in agreement with the location of the critical point calculated within DMFT. For a semi-elliptic density of states the critical values are $U_c \simeq 11.7$ and $T_c \simeq 0.127$ [24], converted to our units which is by a factor of more than two below the maximum Néel temperature *i.e.* deep inside the antiferromagnetic phase.

4 Conclusions

We have performed QMC simulations of the half-filled 3D Hubbard model on simple cubic lattices of up to 10^3 sites. Using finite-size scaling of the magnetic structure factor it is shown that the low-temperature maximum of the specific heat coincides with the antiferromagnetic phase transition. The Néel temperature thus obtained interpolates smoothly between the analytic solutions for weak and strong coupling but differs significantly from the results of previous QMC simulations. The shape of the specific heat curves close to the phase transition is similar to the one obtained for the 3D spin 1/2 Heisenberg model using high precision QMC simulations [21] indicating that both models are in the same universality class. There is no indication of a first-order transition for small values of U contrary to a conjecture established in previous QMC simulations [4,5].

In order to investigate the transition from metallic to insulating behavior in the paramagnetic phase above T_N we have calculated the electronic compressibility. The transition appears to be broadened in accordance with the crossover scenario developed in the framework of the DMFT. For $T = 0.45$ the crossover regime extends over the range $9 \lesssim U \lesssim 11$ which is somewhat below what is obtained in DMFT calculations [25].

It would be very interesting to perform QMC simulations for a Hubbard model where antiferromagnetism is suppressed by adding a next-nearest neighbor hopping t' in order to confirm the existence of the first order transition line obtained within the DMFT. It is however to be feared that in this case the notorious minus sign problem will prohibit efficient QMC simulations at low enough temperatures. We estimate that the average sign of the fermion determinant behaves as $\propto \exp(-\beta t')$ which means that for temperatures of the order of t' the minus sign problem becomes severe and therefore the development of improved QMC algorithms is needed to study this problem.

We thank P. van Dongen and P. Schwab for useful discussions. This work was supported by the DFG as a part of the project *metal-insulator transition and magnetism in highly correlated transition-metal chalcogenids* (HO 955/2).

References

1. M.C. Gutzwiller, Phys. Rev. Lett. **10**, 159 (1963).
2. J. Hubbard, Proc. Roy. Soc. London, Sect. A **276**, 238 (1963).
3. J. Kanamori, Prog. Theor. Phys. **30**, 275 (1963).
4. J.E. Hirsch, Phys. Rev. B **35**, 1851 (1987).
5. R.T. Scalettar, D.J. Scalapino, R.L. Sugar, D. Toussaint, Phys. Rev. B **39**, 4711 (1989).
6. M. Ulmke *et al.*, Phys. Rev. B. **54**, 16523 (1996).
7. Y. Kakehashi, P. Fulde, Phys. Rev. B **32**, 1595 (1985); Y. Kakehashi, J.H. Samson, Phys. Rev. B **33**, 298 (1986).
8. P.G.J. van Dongen, Phys. Rev. Lett. **67**, 757 (1991); Phys. Rev. B **50**, 14016 (1994).
9. Y.H. Szczech, M.A. Tusch, D.E. Logan, Phys. Rev. Lett. **74**, 2804 (1995).
10. M. Jarrell, Phys. Rev. Lett. **69**, 168 (1992).
11. A. Georges, W. Krauth, Phys. Rev. B **48**, 7167 (1993).
12. M. Ulmke, V. Janis, D. Vollhardt, Phys. Rev. B **51**, 10411 (1995).
13. A.-M. Daré, G. Albinet, Phys. Rev. B **61**, 4567 (2000).
14. A. Singh, Eur. Phys. J. B **11**, 5 (1999).
15. G.S. Rushbrooke, G.A. Baker, P.J. Wood, in *Phase Transitions and Critical Phenomena*, edited by C. Domb, M.S. Green (Academic Press, New York, 1974), Vol. 3.
16. H. Hasegawa, J. Phys. Cond. Matt. **1**, 9325 (1989).
17. N.F. Mott, *Metal Insulator Transitions* (Taylor & Francis, 1974).
18. For a review see A. Georges, G. Kotliar, W. Krauth, M.J. Rozenberg, Rev. Mod. Phys. **68**, 13 (1996).
19. R. Blankenbecler, D.J. Scalapino, R.L. Sugar, Phys. Rev. D **24**, 2278 (1981).
20. J.E. Hirsch, R.L. Sugar, D.J. Scalapino, R. Blankenbecler, Phys. Rev. B **26**, 5033 (1982).
21. A.W. Sandvik, Phys. Rev. Lett. **80**, 5196 (1998).
22. R. Staudt, M.Dzierzawa, A. Muramatsu, Ann. Phys. (Leipzig) **8**, SI-249 (1999).
23. R. Staudt, doctoral thesis, Univ. Augsburg (1999).
24. M.J. Rozenberg, R. Chitra, G. Kotliar, Phys. Rev. Lett. **83**, 3498 (1999).
25. Th. Pruschke, D.L. Cox, M. Jarrell, Phys. Rev. B **47**, 3553 (1993).